Materials Today Advances 28 (2025) 100666

Contents lists available at ScienceDirect

Materials Today Advances

journal homepage: www.journals.elsevier.com/materials-today-advances/

Dimethylacrylamide-based gels for expansion microscopy across different solvents

Murilo Izidoro Santos [a], Zviadi Katcharava [b,c], Prerak Dhawan [a], Tobias Hedkte [d], Wolfgang H. Binder [b,c], Christian E.H. Schmelzer [d], Sébastien Blaise [e], Ralf B. Wehrspohn [a], Juliana Martins de Souza e Silva [a,b,*]

[a] Microstructure-based Material Design, Institute of Physics, Martin Luther University Halle-Wittenberg, 06120, Halle, Germany
[b] Design of 3D-Printable Polymers Based on Regional Resources, Just Transition Center, Martin Luther University Halle-Wittenberg, 06099, Halle, Germany
[c] Macromolecular Chemistry, Institute of Chemistry, Martin Luther University Halle-Wittenberg, 06120, Halle, Germany
[d] Fraunhofer Institute for Microstructure of Materials and Systems IMWS, 06120, Halle, Germany
[e] UMR CNRS 7369 MEDyC, University of Reims Champagne-Ardenne, 51100, Reims, France

ARTICLE INFO

Keywords:
Expansion microscopy
Gel embedding
Hydrogel
Organogel
Fluorescence microscopy
Tropoelastin

ABSTRACT

Expansion microscopy (ExM) enables super-resolution visualization using standard light microscopes. Recent developments have explored dimethylacrylamide (DMAA) to improve gel robustness, but compatibility with organic solvents remains a challenge. This study presents a novel hydrogel formulation based solely on DMAA that omits acrylamide (AA) and sodium acrylate (SA): This formulation achieves superior mechanical properties and is compatible with a range of solvents, including ethanol, isopropanol, and acetone. Using eosin-stained tropoelastin fibers as a model, we demonstrated that the gel preserves structural integrity and achieves tunable linear expansion factors of 2.0 ± 0.1-fold in water and ethanol, 1.9 ± 0.1-fold in isopropanol, and 1.6 ± 0.1-fold in acetone. We validated the protocol using dense murine aortic tissue, achieving a 2.0-fold expansion, which successfully resolved fine architectural details that were unresolvable in the native tissue at the same magnification. Furthermore, we found that expanding ethanol-based eosin-stained samples improves imaging contrast compared to the aqueous protocol. By enabling high-fidelity imaging of biological samples in diverse solvent environments, this DMAA-based gel system substantially broadens the applicability of ExM, opening new possibilities for integrating it with complex labeling workflows requiring organic solvents and enabling future correlative microscopy studies across multiple imaging platforms.

1. Introduction

Expansion microscopy (ExM) is a cutting-edge imaging method that enables super-resolution visualization of biological samples using standard light microscopes [1–3]. The technique is based on the isotropic expansion of a polymeric hydrogel network embedded within the biological specimen, causing features in the sample to physically enlarge and separate, allowing resolution at a scale beyond the diffraction limit of light [4]. Conventional ExM protocols expand samples 4–10 fold linearly, translating to a 64–1000 fold volumetric increase [1,5–9], while more recent protocols use optimized hydrogel chemistries to achieve linear expansion factors of up to 20-fold, potentially enabling nanoscale resolution as fine as 20 nm [10]. Such methods rival the resolution of advanced techniques like STED and STORM [11], making ExM particularly valuable for multi-color imaging and detailed studies of cellular ultrastructure, including synaptic organization and organelle morphology.

The ExM procedure consists of several sequential stages. Typically, the structures of interest within the sample are labeled using fluorescent markers to enable visualization of specific biomolecules, such as proteins [12–16], nucleic acids [17–19], carbohydrates [17,18] and lipids [3,17,20]. Next, the sample's biomolecules are anchored to the hydrogel network through covalent bonds, ensuring that the spatial arrangement of these biomolecules remains intact during the expansion process. Following this, the hydrogel is polymerized within the sample, creating a crosslinked polymer matrix. The sample is then digested using detergents [12] or enzymes [1] to break down protein-protein interactions, facilitating uniform expansion of the embedded specimen. Immersion in

* Corresponding author. Microstructure-based Material Design, Institute of Physics, Martin Luther University Halle-Wittenberg, 06120, Halle, Germany.
E-mail address: juliana.martins@physik.uni-halle.de (J.M. de Souza e Silva).

https://doi.org/10.1016/j.mtadv.2025.100666
Received 27 May 2025; Received in revised form 28 October 2025; Accepted 14 November 2025
Available online 21 November 2025

water or a low-salt buffer induces isotropic swelling of the hydrogel, expanding the sample while maintaining structural fidelity. Finally, the expanded sample is imaged using standard light microscopy techniques, and the results are validated by comparison with known standard protocols [8,21].

The hydrogel formulations used in ExM typically consist of acrylamide (AA), sodium acrylate (SA), and N,N′-methylenebisacrylamide (MBA) that are covalently linked through free-radical polymerization of vinyl groups. Acrylamide serves as the primary backbone of the polymer matrix, offering structural integrity, while MBA acts as a crosslinker, stabilizing the network by connecting polymer chains. Sodium acrylate introduces ionic groups that increase hydrogel swelling in aqueous media required to achieve high volumetric expansion factors [8,9]. Optimization of the gel composition is a critical aspect of all ExM protocols. Factors such as the crosslinker-to-monomer ratio are carefully adjusted to improve the swelling properties of the hydrogel while preserving its mechanical stability [22]. This adjustment ensures that the gel remains robust enough for easy preparation and safe handling throughout the experimental workflow, contributing to consistent results across different applications of ExM.

Recent developments on ExM protocols have explored dimethylacrylamide (DMAA) either in combination with [6,23] or as a substitute for AA [10,24,25]. One of the advantages of using DMAA in gel formulations is due to its ability to self-crosslink through methyl groups during heat treatment, in addition to crosslinking via vinyl groups [26]. This dual crosslinking mechanism promotes a more uniform crosslink distribution within the gel's network, resulting in a more robust gel with minimized risk of distortions induced by crosslinking artifacts [27]. This principle was explored by Truckenbrodt et al. [28] in the X10 protocol, which was the first ExM iteration to incorporate DMAA into its composition, achieving up to a 10-fold expansion in a single-step process. Furthermore, DMAA is a less polar molecule than AA, making it compatible with solvents of lower polarity than water [29]. Thus, replacing AA with DMAA has the potential to increase the versatility of ExM by enabling the use of expanded samples in alternative, non-aqueous solvents. This, in turn, may broaden the applicability of ExM to samples and experimental protocols that require compatibility with specific solvent environments. For instance, in electron microscopy (EM), water-swollen gels are incompatible with the low-pressure conditions necessary for imaging. Moreover, transmission imaging of soft materials often relies on ultrathin sectioning, typically achieved by microtomy of specimens embedded in resins with very low water tolerance. Similarly, in techniques such as X-ray microscopy (XRM/micro-CT), exposure of soft tissues to high-energy beams can lead to bubble formation or cavitation [30]. In such cases, dehydration and subsequent stabilization of the specimens within resin matrices may be advantageous. While re-embedding strategies have been developed to stabilize water-expanded gels by locking them in a secondary, non-expanding polyacrylamide matrix, thereby preventing shrinkage in high-salt environments [31] and maintaining mechanical integrity for iterative expansion protocols [32], these approaches are not compatible with non-aqueous solvents. This limits their utility for workflows requiring direct compatibility with organic solvent-based staining and processing protocols essential for electron microscopy (EM) or X-ray microscopy.

In this work, we developed a novel hydrogel formulation based on DMAA that not only expands in water, but is also compatible with organic solvents, including ethanol, isopropanol, and acetone. It maintains robust mechanical properties at a modest expansion across the different solvents tested. Particularly, ethanol-expanded DMAA gels enhanced the resolution of eosin-stained tropoelastin and mouse aorta tissue under standard fluorescence microscopy, demonstrating the imaging advantages and broader applicability of this method.

2. Materials and methods

2.1. Materials

All chemicals used in this study are listed in Table S1 in the supplementary material. Stock solutions were prepared whenever necessary to streamline gel preparation. The stock concentrations and storage conditions are listed in Table S2.

2.2. Development and optimization of DMAA-based gel formulations

2.2.1. Preparation of gel formulations

To prepare the formulations, the required quantities of DMAA, deionized water, and stock solutions of AA 60 wt%, MBA 2.5 wt%, PBS 0.1 mol L^{-1}, and methacrolein 5 wt% (Table S3) were measured into a glass vial. The gel precursor could either be stored at 4 °C for future use or used immediately after adding VA044 initiator from a 25 wt% stock solution. A series of formulations with varying amounts of DMAA (5, 10, 15, 20, and 25 wt%) and AA (20, 15, 10, 5, and 0 wt%) in the presence of a final concentration of 0.1 wt% MBA was prepared (Table S3). Each sample was named according to the weight ratio DMAA:AA:MBA in the formulation (e.g., sample labeled 15:10:0.1 contained 15 wt% DMAA, 10 wt% AA and 0.1 wt% MBA). Similarly, formulations with DMAA 25 wt%, without AA, and varying ratios of the crosslinker MBA (0.025, 0.031, 0.05, and 0.1 wt%) were prepared (Table S4) (e.g., sample labeled 25:0:0.1 has 25 wt% DMAA, no acrylamide and 0.1 wt% MBA). As an example, to prepare 5 g of a gel solution with a final concentration of 25 wt% DMAA, 0 wt% AA and 0.1 wt% MBA (i.e., sample 25:0:0.1), 1.25 g DMAA, 0.2 g MBA (2.5 wt% stock solution), 0.5 g PBS (0.1 M stock solution), 0.25 g methacrolein (5 wt% stock solution) and 2.75 g of deionized water were measured into a 10 mL glass vial. To activate the solution for polymerization, 0.05 g of VA044 (25 wt% stock solution) were added to the vial.

2.2.2. Gel polymerization and swelling tests of DMAA-based gels in different solvents

Gel formulations (ca. 5 g) were degassed under vacuum in ultrasonic bath for ca. 15 min. Then, aliquots of 200 μL of each formulation (Table S3) were cast into the wells of a 48-well cell plate to create disc-shaped samples of 11 mm diameter and ca. 2 mm height. The plate was then placed inside a glass desiccator containing water at the bottom to maintain the surface hydration of the gels. Vacuum was applied for ca. 15 min to deplete oxygen from the system and eliminate any trapped air bubbles within the casts. Following this, the system was purged with a steady flow of N_2 for 1 min and then closed. The container was transferred to a pre-heated oven set at 50 °C and incubated for 6 h to complete gel polymerization. The resulting disc-shaped gels were carefully removed from the casts and measured using a calliper. Swelling behavior was then evaluated in various solvents. Therefore, all samples were fully expanded by immersion in ca. 25 mL of water for 3 days, with the water being replaced daily to wash away salts and non-crosslinked molecules, for equilibrium swelling in water. Then, the gels' dimensions were measured again. The discs were then transferred to ca. 25 mL of one of the following solvents: ethanol, isopropanol, or acetone, in which they were completely immersed for an additional 3 days, with daily solvent changes, for a final swelling evaluation.

2.2.3. Rheological assessment of gel formulations

An Anton Paar MCR-101 DSO rheometer equipped with parallel plate geometry (d = 25 mm) was used for the rheology measurements. The device was equipped with Peltier temperature control for ensuring accurate temperature control and nitrogen gas purge. The DMAA formulation was quickly loaded onto the preheated rheometer surface at 50 °C, the gap was reduced to 0.15 to 0.18 mm and the measurement was performed at a frequency of 1 Hz. The recorded data were analyzed using RheoCompass™ (V1.34) and OriginPro 2019.

2.2.4. FTIR analysis of DMAA-based gels

FTIR measurements were performed using the attenuated total reflection technique on a VERTEX 70 v FT-IR Spectrometer (Bruker) equipped with the golden gate diamond ATR unit. Measurements were conducted at room temperature in the spectral range of 4000–550 cm^{-1}. Data analysis was performed using Opus 8.2 and OriginPro 2019.

2.2.5. Compression tests of DMAA-based gels in different solvents

To assess the mechanical properties of the DMAA-based gel formulations, the DMAA gels (Table S4) and reference gels (Table S5) were cast into a 48-well cell plate by dispensing approximately 1.5 mL of the mixture into each well, producing cylinder-shaped samples with a diameter of 11 mm and a height of approximately 15 mm. The gels were polymerized, carefully removed from the casts, and measured using a caliper for additional evaluation of the swelling behavior. Gel samples were divided into two groups for evaluation in the swollen state. The first group underwent compression testing after six days of immersion in water, while the second group was tested after immersion for three days in water, followed by an additional three days in ethanol, isopropanol or acetone. Swollen gels in both groups were subjected to uniaxial compression until rupture at a strain rate of 0.1 mm/s in a TA.XT Texture Analyzer (TA.XTplus, Stable Micro Systems, Godalming, SRY, UK). The compressive modulus was calculated from the linear region of the stress-strain curves, specifically within the strain range of 0.1 % to 2 %, for all samples. Additionally, stress and strain at break were recorded. Each measurement was conducted with a sample size of $n \geq 4$.

2.3. Application of the DMAA-based gels for the expansion of tropoelastin samples

2.3.1. Tropoelastin electrospun mat preparation

Tropoelastin derived from *E. coli* [33] was dissolved in hexafluoroisopropanol (HFIP) to a concentration of approximately 9 wt%. The solution was electrospun using an LE-50 unit (Fluidnatek, Valencia, Spain) at a flow rate of 0.5 mL h^{-1}, with an applied voltage of 18 kV. Fibers were collected on a polypropylene substrate positioned 12 cm from the spinneret over a duration of 15 min. The samples were then dried overnight at 30 °C and subsequently crosslinked in a formaldehyde-saturated atmosphere for 90 min, as described elsewhere [34].

2.3.2. Staining of tropoelastin fibers before expansion

A 0.1 wt% eosin Y solution was prepared in PBS (0.01 M, pH 7.4), filtered using a 0.2 μm syringe filter, and stored at 4 °C. Tropoelastin samples were cut into rectangles (1 mm × 2 mm), with one edge bearing an angular incision to aid orientation. Samples were placed onto clean glass slides and stained by overlaying 10 μL of 0.1 wt% eosin Y in PBS for 1 h at ambient temperature. Afterwards, samples were rinsed three times with a 1:1 (v/v) ethanol:water mixture and the solution was removed using a wipe to prevent loss or disruption of the sample. After rinsing, the samples were air-dried for 1 h. A coverslip was mounted atop each sample and secured with tape for a subsequent imaging step.

2.3.3. Embedding of tropoelastin fibers in DMAA-based gel

A solution was prepared by adding 1.25 g DMAA, 2.9 g deionized water, 0.05 g MBA 2.5 wt%, 0.5 g PBS 0.1 mol L^{-1}, and 0.25 g methacrolein 5 wt% (Table S2) into a 10 mL glass vial to obtain a final ratio of DMAA:AA:MBA equal to 25:0:0.025. The resulting solution was filtered through a 0.2 μm syringe filter and could be stored for up to 2 weeks after preparation. Then, 0.05 g of VA044 25 wt % was added, and the solution was purged with a steady flow of N_2 for 5 min, then degassed under vacuum in an ultrasonic bath. The tropoelastin samples (1 mm × 2 mm) were mounted in a custom-built gelation chamber (Fig. S1). Then, 100 μL of the previously prepared solution was added to each chamber and transferred to a glass desiccator containing water at the bottom to prevent dehydration of the gel during polymerization. To deplete oxygen from the sample environment, a vacuum was applied for 15 min, followed by 1 min of N_2 purging. The desiccator was closed, and the samples were incubated overnight at room temperature, then transferred to a preheated oven at 50 °C for 6 h to complete polymerization.

2.3.4. Expansion of tropoelastin fibers in DMAA-based gel

Samples embedded with the DMAA-based gel were trimmed in a trapezoidal shape to facilitate the subsequent imaging steps. Then, a solution containing 200 mM sodium dodecyl sulfate (SDS), 200 mM sodium chloride, and 50 mM Tris-HCl, was added and adjusted to pH 9. Digestion was carried out at 80 °C for 60 h. After digestion, the gels were transferred to PBS 0.01 mol L^{-1} solution (pH 7.4) and rinsed overnight for neutralization and removal of SDS. The samples were then placed in water for an additional 24 h to allow full expansion.

2.3.5. Post-expansion staining

Tropoelastin fibers expanded in the DMAA-based gel in water were immersed in 0.01 wt% eosin Y solution (PBS, pH 7.4) for 1 h at room temperature. After staining, the samples were rinsed overnight in deionized water, then the water was replaced three times every 1 h to ensure thorough removal of excess stain. After imaging, the solvent was gradually changed over 24 h to either ethanol, isopropanol or acetone in a series of solutions (50 %, 70 %, then 2 × 100 %).

2.3.6. Imaging of tropoelastin mats

The samples were imaged using a fluorescence microscope (BZ-X800, Keyence Corp., Osaka, JP), equipped with a high-intensity LED light source covering the UV–IR spectral range. The fluorescence emission range was selected by inserting the appropriate filter into the optical path of the objective lens. Full-sample images were acquired with a PlanApo 4x objective lens (NA 0.2) in bright-field mode at 1/300 s. For higher magnification, regions of interest (ROIs) were imaged at the TxRed channel (red fluorescence) using a PlanApo 40x objective (NA 0.95) at an exposure time of 1/70 s, from which full-focus images were reconstructed from Z-stacks captured at a pitch of 0.4 μm. Following expansion in DMAA-based gels, the stained tropoelastin specimens were transferred to a 6-well cell culture plate, immersed in the corresponding solvent (water, ethanol or isopropanol). Due to the incompatibility of the cell plate polymer with acetone, acetone-expanded samples were placed in glass petri-dishes filled with acetone and hermetically sealed with BluTack (Bostik Inc., Colombes, France). Fluorescence images of expanded samples were acquired with a PlanApo 4x objective (NA 0.2) at a 1/1.2 s exposure time. Full-focus images were composed from Z-stacks acquired at a 20 μm pitch. ROIs were then magnified using a PlanApo 20x objective (NA 0.75) at exposure times between 1/7.5 s to 1/5 s, depending on the solvent used for expansion, creating full-focus images from Z-stacks acquired at a pitch of 5 μm. Local expansion factors and image resolution were assessed on ImageJ (v1.54p, NIH, USA) by comparing line profiles drawn between corresponding features on regions of interest (ROIs) in images acquired at three stages: pre-expansion, post-expansion in water, and after changing the expansion medium to ethanol, isopropanol, or acetone, respectively.

2.3.7. Fluorescence retention rate of samples pre- and post-expansion in expansion microscopy

Fluorescence imaging was performed on a BZ-X800 fluorescence microscope (Keyence Corp., Osaka, JP), pre- and post-expansion using the same acquisition settings (4 × magnification, both brightfield and red fluorescence channels were acquired at exposure times of 1/2.5 s. Z-stacks were collected with 3 μm intervals). Fluorescence intensity was quantified using ImageJ by defining ROIs, and measuring the mean fluorescence intensity in pre- and post-expansion images. Dilution due to sample expansion and potential fluorescence loss was normalized by correcting for pixel size differences after expansion using Eq. (1):

$$Intensity_{normalized} = \frac{Intensity_{measured}}{Expansion\ Factor^3} \quad \text{Eq. (1)}$$

The total fluorescence was background corrected, and the fluorescence retention rate is determined using Eq. (2):

$$Retention\ Rate\ (\%) = \left(\frac{Post - expansion\ Fluorescence}{Pre - expansion\ Fluorescence}\right) \times 100 \quad \text{Eq. (2)}$$

using background-subtracted, normalized intensity values. The measurement was repeated across several regions of the sample and is reported with the standard deviation.

2.4. Application of the DMAA-based gels for the expansion of mouse aorta

2.4.1. Sample description

The 4-month-old, healthy, wild-type mouse aorta used in this study were obtained from an animal that was maintained under standard laboratory conditions with ad libitum access to food and water until the time of sacrifice (Ethics Committee for Animal Welfare of the University of Reims Champagne-Ardenne, CEEA-RCA No. 56). The aortas were carefully dissected under a stereomicroscope to avoid mechanical damage, rinsed in cold phosphate-buffered saline (PBS) to remove blood, and then fixed in 4 % paraformaldehyde. After fixation, the tissues were dehydrated using a graded ethanol series, cleared in xylene, and embedded in paraffin for subsequent sectioning at a thickness of 7 μm using a rotating microtome (HM 355, Microm, Walldorf - DE) and mounted onto glass slides. For staining, the sections were deparaffinized in xylene (2 × 10 min), rehydrated through a graded ethanol series (3 × 100 %, 2 × 96 %, 85 %, 70 %; 3 min each), and rinsed in distilled water for 20 s. Hematoxylin and eosin (H&E) staining was performed by immersing the sections in Mayer's hematoxylin solution for 1 min, rinsing in water, and bluing in 0.1 wt% sodium bicarbonate solution. Slides were then counterstained with a 0.2 wt% ethanolic eosin solution for 1 min, rinsed in water and covered with a 1.0# cover glass by depositing 100 μL of a 85 vol% glycerol solution for imaging.

2.4.2. Pre-expansion imaging of mouse aorta

Stained sections of mouse aorta were imaged using a fluorescence microscope (BZ-X800, Keyence Corp., Osaka, Japan). Full-sample images were acquired with a Plan Apo 4 × objective (NA 0.2) in bright-field mode at a 1/350 s exposure and in red fluorescence mode using a TxRed filter at a 1/1.2 s exposure. Each final image was generated by stitching a 2 × 3 grid of individual fields. ROIs were imaged with a Plan Apo 40 × objective (NA 0.95) using a TxRed filter at a 1/35 s exposure. Full-focus images were reconstructed from Z-stacks captured at 1 μm intervals.

2.4.3. Embedding of mouse aorta sections in DMAA-based gel

Following the imaging process, the coverslips were removed by submerging the slides in water, followed by 15 sequential rinses in fresh water to eliminate excess glycerol. The residual water surrounding the tissue sections was gently absorbed using a lint-free paper wipe. Subsequently, a gelation chamber was constructed around the sections by placing two stacks of #1.0 coverslips on opposite sides of the slide, securing them in position with superglue. The gelation chamber was sealed with a cover glass that has been wrapped in parafilm. The slide containing the gelation chamber was then maintained at 4 °C prior to embedding. In parallel, a fresh gel solution was prepared by combining 0.5 g of DMAA, 1.16 g of deionized water, 0.02 g of MBA (2.5 wt%), 0.2 g of PBS (0.1 mol L^{-1}), and 0.1 g of methacrolein (5 wt%) in a 5 mL glass vial (DMAA:AA:MBA ratio of 25:0:0.025). The solution was purged with a steady flow of nitrogen for 5 min, then degassed under vacuum in an ultrasonic bath for 10 min in the presence of ice. Subsequently, 2 μL of 1 wt% 4-hydroxy TEMPO (4-HT), 8 μL of 10 wt% N,N,N′,N'-tetramethylethylendiamine (TEMED), and 40 μL of 10 wt% ammonium persulfate (APS) were added to the vial under ice. The samples were embedded in the gel solution by carefully filling the gelation chamber with approximately 200 μL of the solution to prevent bubble formation. The slides containing the gelation chamber were then placed in a pre-cooled vacuum-resistant container. A vacuum was applied to the system for 2 min, followed by a 1 min purge with nitrogen to remove oxygen from the container. Finally, the system was incubated for 2 h at 4 °C, after which the gel was polymerized at 37 °C for 6 h.

2.4.4. Digestion and expansion of mouse aorta

Samples embedded in the DMAA-based gel were trimmed into a trapezoidal shape to facilitate subsequent imaging steps. The samples were then transferred to 10 mL glass vials containing 2 mL of a solution composed of 200 mM sodium dodecyl sulfate (SDS), 200 mM sodium chloride, and 50 mM Tris-HCl, adjusted to a pH of 9. The digestion process was conducted at 80 °C for 60 h, with the solution being replaced every 24 h. After digestion, the gels were briefly rinsed with deionized water and incubated overnight in 50 mL of a 0.01 mol L^{-1} PBS solution (pH 7.4) to neutralize and remove SDS. The samples were then subjected to three incubations in approximately 50 mL of water for 8 h to achieve full expansion. Finally, the samples were incubated overnight in 1 vol% acetic acid to improve eosin Y staining.

2.4.5. Post-expansion staining of mouse aorta

The samples were incubated in water for 1 h, followed by staining in 3 mL of a 0.1 wt% eosin Y solution in PBS (0.01 M, pH 7.4) for an additional 1 h. After staining, the samples were rinsed in water until no eosin Y residue was visible from the washes.

2.4.6. Post-expansion imaging of mouse aorta

Samples were transferred to a petri dish and kept immersed in water after staining. For imaging, excess water was removed to ensure proper placement of the sample on the coverslip. Samples were imaged using a fluorescence microscope (BZ-X800, Keyence Corp., Osaka, Japan) in fluorescence mode (TxRed filter). Whole-sampe images were acquired using a PlanApo 4x objective (NA 0.2) at 1/1.2 s exposure time. Full-focus images were generated from Z-stacks acquired at a pitch of 48 μm through stitching a 4 × 6 grid of individual fields. ROIs in the sample were visualized with a PlanApo 10x objective lens (NA 0.45) at 1/6 s exposure time. Full-focus images were generated from Z-stacks acquired at a pitch of 20 μm. For higher magnifications, the ROIs were imaged with a PlanApo 20x objective lens (NA 0.75) in fluorescence mode (TxRed filter) at 1/2 s exposure time. Full-focus images were generated from Z-stacks acquired at a pitch of 10 μm. After imaging, the expansion medium was changed by incubating the samples three times in excess absolute ethanol (two times for 6 h, then overnight) without detaching the sample from the bottom of the Petri dish. The imaging process was then repeated using the same parameters as those used for imaging in water to ensure comparability between the images.

2.5. Distortion analysis

To quantify the spatial distortions introduced by the expansion process, image registration was performed between pre- and post-expansion images of each sample for the same field of view. First, the pre- and post-expansion images were aligned through rigid-body registration using Scale Invariant Feature Transform (SIFT) in ImageJ. The transformation matrix obtained from this process provided a global estimate (over the region of interest) on the expansion factor required to align the pre- and post-expansion images within the region of interest. The resulting set of aligned images (the upscaled pre-expansion image and its post-expansion counterpart) were then non-rigidly registered using the optical flow algorithm to compute the displacement field between the reference image (before expansion) and the target image (after expansion in solvents) [46]. This method has previously been used to evaluate the relative shifts of characteristic features in the pre- and

post-expansion images [47]. The resulting local displacement vectors were then used to calculate the root-mean-square error (RMSE) of the pairwise distances of specific features in the image set, as a function of the measuring distance. To do this, 10^5 pairs of points were randomly chosen on a binarized skeleton of the post-expansion image, and the corresponding distance was measured in the pre-expansion image. The differences in these lengths were then binned to calculate the RMSE as a function of observation distance in the pre-expanded state (lengths before rigid registration), providing a measure of local distortions throughout the entire process.

2.6. Statistical tests

Means comparison tests of compressive Young's modulus, strain at break, and of expansion factors measured from microscopy images were conducted in OriginPro 2019 using Tukey's (honestly significant difference - HSD) test at a significance level of 0.05.

3. Results and discussion

3.1. Development and optimization of DMAA-based gel formulations

Our research focused on gel formulations based on dimethylacrylamide (DMAA), chosen for its compatibility with both water and solvents of lower polarities [29,35]. Unlike other ExM protocols that use DMAA-based gels [6,24,36], we started our approach by omitting sodium acrylate (SA) from the formulations. The aim of this adjustment was to change the polarity profile of the gels by the removal of the more polar molecule. We explored alternative gel formulations with DMAA alone or copolymerized with AA in a neutral aqueous medium to form the polymer backbone (Fig. 1). To create the three-dimensional network essential for gel expansion, a bifunctional vinylated crosslinker (N, N'-methylenebisacrylamide – MBA) was incorporated into the formulations. To initiate the polymerization, we utilized the thermal initiator VA044, instead of the commonly used persulfate/TEMED system. The choice of VA044 allowed gelation to begin at a higher temperature (at ca. 50 °C), enabling incubation of the precursor solution with the sample

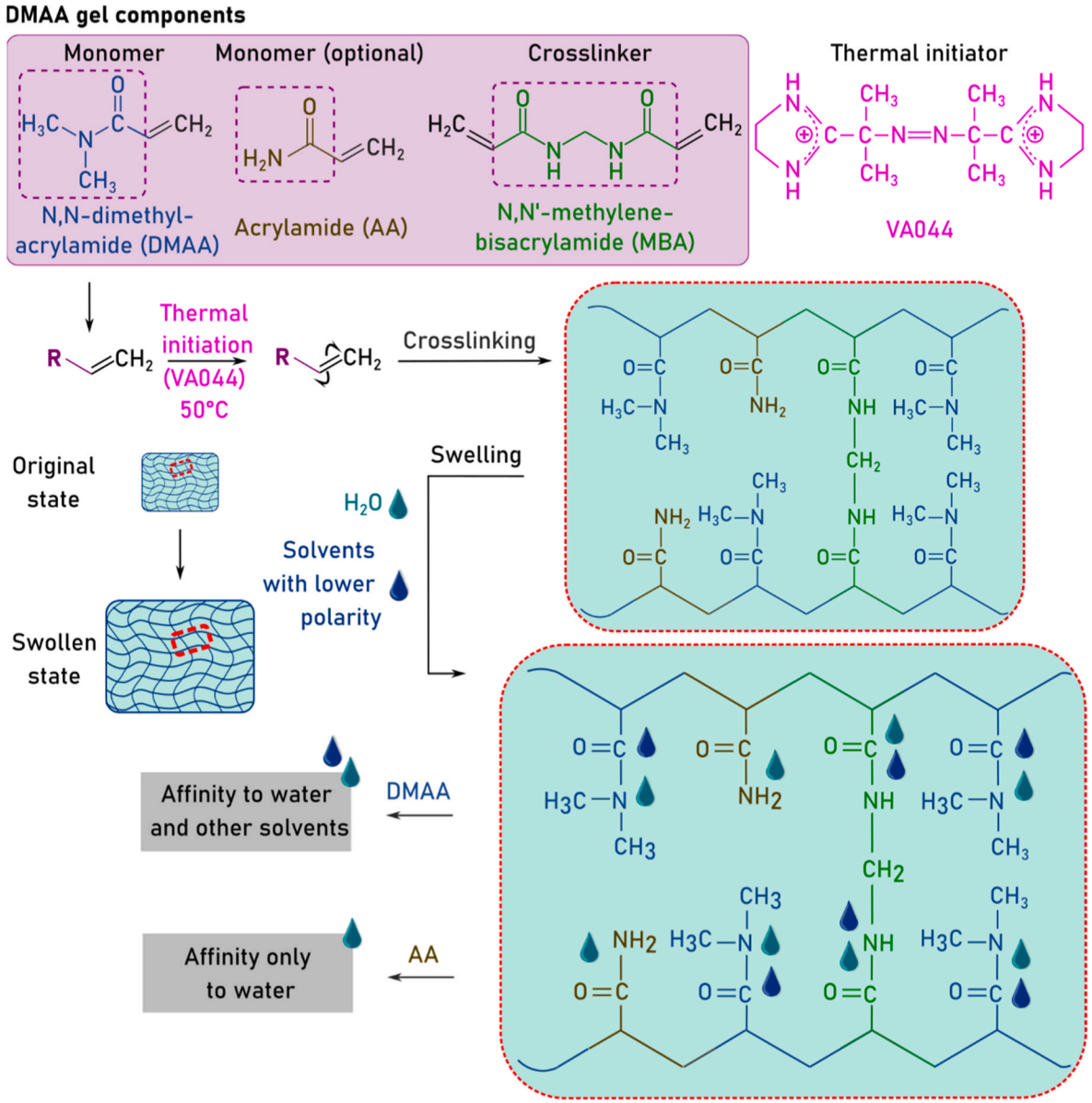

Fig. 1. Schematic representation of the thermal crosslinking of DMAA-based gels containing different amounts of AA and MBA and their subsequent swelling in different solvents.

at room temperature. This approach simplified the proposed expansion workflow by facilitating monomer diffusion into the sample while avoiding undesired precipitation of components of the gel precursor solution at low temperatures. Due to the high sensitivity of VA044 to oxygen in the crosslinking (gelation) process, we purged the solution with nitrogen while simultaneously applying vacuum and ultrasound to degas it. Once crosslinked, the polymer network could be exposed to water or other solvents with affinity to its components, causing the network to swell due to osmotic effects [37].

We prepared disk-shaped gels without a sample to investigate the influence of adjusting the ratio of DMAA to AA and MBA in the gel formulation on the gel's compatibility with different solvents. After crosslinking and extracting salts from the gels in water, we systematically tested their ability to remain expanded when immersed in one of the following solvents, ranked in order of decreasing polarity: ethanol, isopropanol and acetone [38]. Measurements of the disk diameters before and after swelling show that the expansion occurs at different rates for different DMAA:AA:MBA ratios and the different solvents (Fig. 2 A, Fig. S2). All gels exposed to water, despite being synthesized with different DMAA:AA:MBA ratios, show similar linear expansion of ca. 1.8-fold, equivalent to 80 % increase in all dimensions, or 5.8-fold in volume. For gels exposed to ethanol and isopropanol, a reduction of AA content or its complete absence in the formulations is beneficial to the expansion: gel formulations of DMAA:AA:MBA ratios equal to 20:5:0.1 and 25:0:0.1 (Fig. 2 A) swell in ethanol and isopropanol as much as when exposed to water. Swelling in acetone shows to be more sensitive to the AA content, and only the sample without AA expanded (1.4-fold) after immersion in this solvent.

We measured the linear expansion of the gels to further investigate the effects of the absence of AA and of changing the DMAA:MBA ratio on the expansion and stability of the crosslinked gels in the different solvents (Fig. 2 B). Gels prepared using the established formulations from the ExM protocol [1] and the MAP protocol [13] exhibit expansion factors greater than 3.6-fold in water. However, as expected from their high contents of SA and AA, these formulations shrink or collapse in other solvents (Fig. S3). In contrast, gels synthesized without AA show more consistent swelling across the tested solvents, albeit with substantially lower expansion factors of around 2-fold. Further reducing the

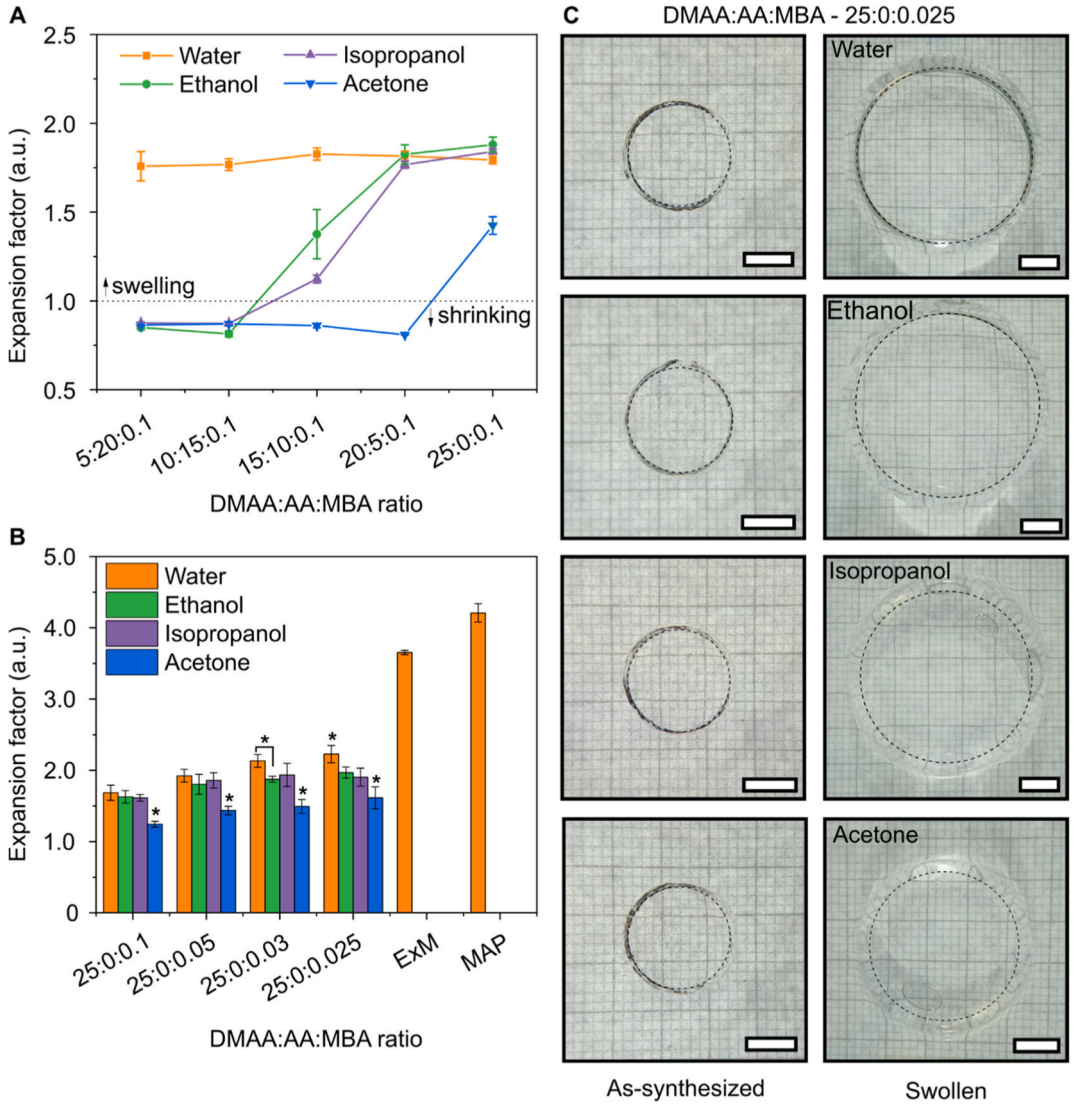

Fig. 2. Gels synthesized under variable ratios of DMAA, AA and MBA and swollen in different solvents. (A) Linear expansion factors of a series of gels with different ratios of DMAA:AA:MBA exposed to water, ethanol, isopropanol, or acetone, (B) linear expansion factors of AA-free gels (variable DMAA:MBA ratios) after swelling in water, ethanol, isopropanol, or acetone in comparison to well-established gel formulations, ExM (original ExM protocol [1]) and MAP (method of Magnified Analysis of Proteome [13]) - * symbol indicates statistically significant difference at level 0.05), (C) photographs of AA-free gels in two stages: post-synthesis and swollen in different solvents (scale bar: 5 mm). Dotted lines at the edge of the gels are a to guide the eye.

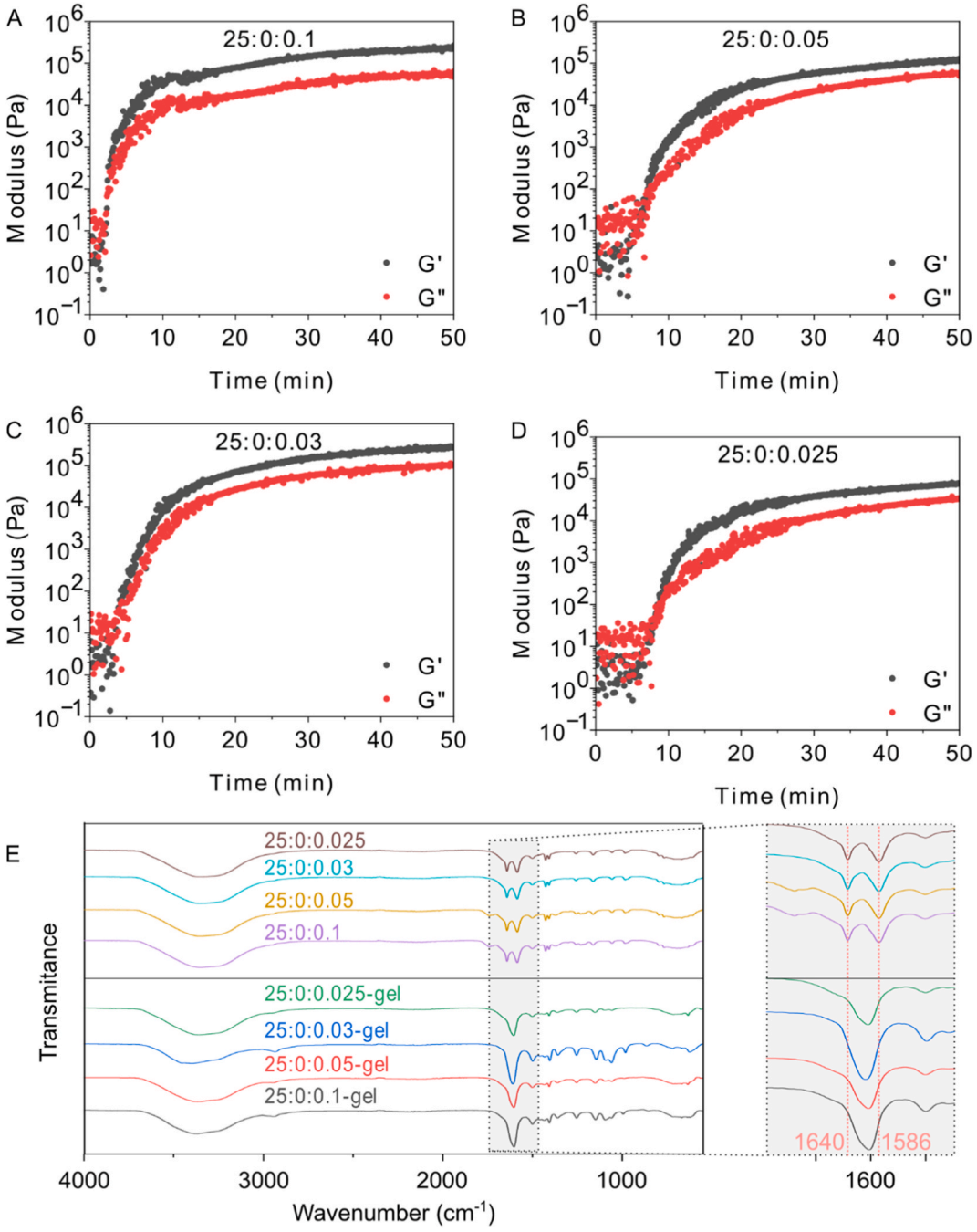

Fig. 3. Rheological analysis of DMAA formulations at 50 °C with varying MBA concentrations: DMAA:AA:MBA of (A) 25:0:0.1, (B) 25:0:0.05, (C) 25:0:0.03, and (D) 25:0:0.025, and (E) FTIR spectra of DMAA formulations and corresponding gels.

crosslinker (MBA) content from 0.1 wt% to 0.025 wt% increases the expansion factor from 1.7-fold to 2.2-fold in water, with similar values observed when the gels are expanded in ethanol or isopropanol. Gels produced with an MBA content lower than 0.025 wt% are unstable and sticky. Similar stickiness was observed in gels produced with a high DMAA content (40 wt%) (Fig. S4). The most expandable and stable gels across the different tested solvents without AA were produced at a ratio DMAA:AA:MBA of 25:0:0.025 (Fig. 2C).

A more detailed characterization of the rheology of the gels (Fig. 3) reveals that the gel point, defined as the crossover between the storage modulus (G') and the loss modulus (G''), occurs at approximately 3 min for the formulation with the highest crosslinker concentration (25:0:0.1, Fig. 3 A). As the crosslinker content decreases, the gel point shifts to ca. 7 min for the formulation 25:0:0.05 (Fig. 3 B), and to ca. 5 min for the formulation 25:0:0.03 (Fig. 3 C). A further reduction in crosslinker content delays the gel point to approximately 9 min (25:0:0.025, Fig. 3 D). These results suggest that decreasing the crosslinker content leads to an increase in the gelation time.

Although the initial modulus values are within the sensitivity range of the instrument, leading to noise in the early part of the measurement, G' and G'' plateau within 50 min as gelation progresses, indicating full monomer conversion for all gels. FTIR spectroscopy (Fig. 3 E) further supports this, as a comparison of the formulations before and after polymerization shows the disappearance of the characteristic C=C stretching vibration ($\nu = 1586$ cm^{-1}) and a shift of the C=O stretching signal from $\nu = 1640$ cm^{-1} to lower values [39,40].

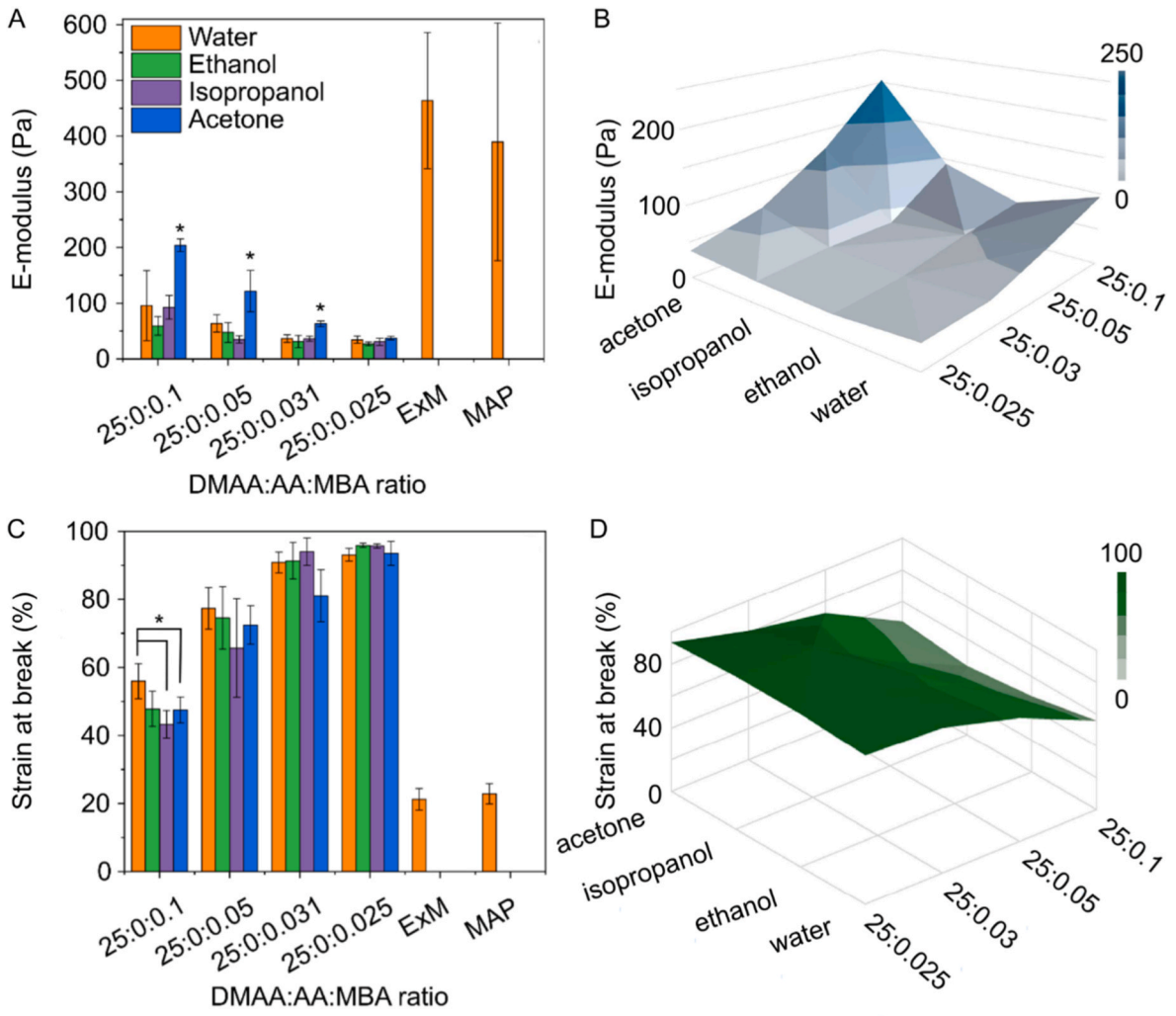

Fig. 4. Mechanical properties of gels prepared in the absence of AA and with varied ratios of DMAA to MBA swollen in four different solvents - water, ethanol, isopropanol and acetone: (A) Compressive Young's moduli, with (B) the respective 3D surface plot; (C) strain at break. (* - statistically significant difference at level 0.05), with (D) its respective 3D surface plot.

The mechanical properties of ExM gels are critical because they determine the gel's ability to undergo uniform and isotropic expansion, maintain structural integrity during handling and imaging, and ensure accurate preservation of spatial relationships within the biological sample. We therefore analyzed the mechanical properties of swollen DMAA:AA:MBA gels prepared at a fixed DMAA concentration (25 wt%) with different MBA concentrations ranging from 0.025 to 0.1 wt% using unconfined compression experiments (Fig. 4). The solvent influences the modulus (Fig. 4 A and B), with acetone generally giving the highest modulus values, indicating a stiffer material. Further reduction of MBA in the formulation will result in less stiff gels in the swollen state, regardless of the solvent. This is understandable as a reduction in crosslinker content generally results in a less rigid polymer network [41]. Compared to the standard protocols, all DMAA-based gels prepared here are less stiff in the swollen state than gels prepared with ExM and MAP. The choice of solvent also affects the strain at break (Fig. 4 C and D) as well as the stress at break (Fig. S5) and as the MBA ratio decreases (25:0:0.1 to 25:0:0.025) the strain at break generally increases for all solvents. This indicates that, regardless of the expansion solvent, the materials become more flexible and can withstand more deformation before breaking when less crosslinker is used and are more resilient during handling. They are more flexible under compressive stress and can deform more before breaking than the gels produced by the ExM and MAP protocols in the swollen state, implying that the DMAA gels are mechanically suitable for expansion microscopy applications.

3.2. *Application of the DMAA-based gels for the expansion of tropoelastin samples*

To establish a proof of principle for expanding elastin-rich biological structures, we first tested a model system of nonwoven electrospun tropoelastin fiber fleeces. For this purpose, we selected the gel formulation (DMAA:AA:MBA 25:0:0.025) that demonstrated the most favorable mechanical properties, namely the highest expansion factor (Fig. 2 B) and the greatest strain at break (Fig. 4 C). Chemically crosslinked tropoelastin was chosen as an example of an insoluble macromolecule that is not easily removed from the tissue during processing, thus providing reliable and relevant experimental dummies. To be able to apply the DMAA gel protocol previously developed to the tropoelastin fiber fleeces, we mounted the fleeces in a gelation chamber (Fig. S1) and incubated them in a gel precursor solution containing monomers and thermal initiator VA044 (Fig. 5). The incubation was performed first at room temperature to facilitate the diffusion of the components, followed by polymerization at 50 °C. Gelation occurred in the presence of methacrolein, which reacts with amine residues, grafting reactive acrylate groups onto proteins via imine bonds [42]. These groups, in turn, polymerize with those in the gel precursor, allowing proteins in the specimens to be anchored directly to the gel, eliminating the need for an

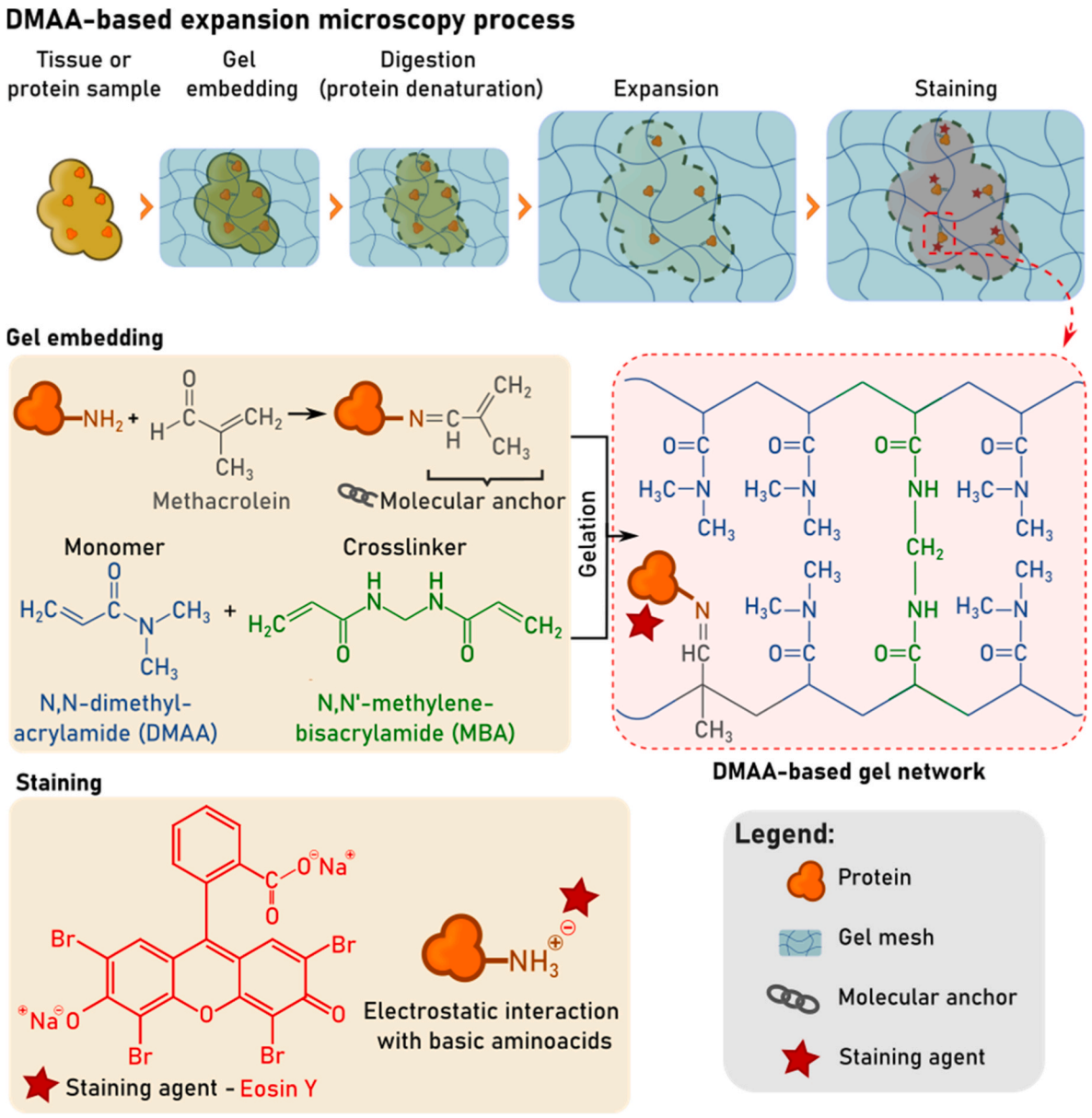

Fig. 5. Experimental scheme of the DMAA-based expansion microscopy process across different solvents highlighting the monomer components used to embed the samples in the gel and the post-expansion staining with eosin Y.

additional incubation step with anchoring agents (e.g., acryloyl-X or label-X) to graft acrylate groups onto proteins, as required in other ExM protocols [12,19]. This simplification reduces laboratory workload and processing time. To ensure uniform expansion of the fleece specimens, we homogenized them using an established protocol based on an alkaline SDS buffer [6,12]. This mild homogenization process effectively preserves the protein content within the specimens, ensuring compatibility with subsequent staining steps following full expansion. The expanded gels were then stained with eosin Y, a widely used histological dye. Eosin Y exhibits intense fluorescence emission at approximately 540 nm in a neutral medium [43] and binds non-specifically to basic amino acid residues arginine, histidine, and lysine [44]. This staining step provides a straightforward method of visualizing the expanded specimens in various solvents by sequentially washing them in the new expansion solvent.

Each of the three tropoelastin fleece samples tested were first expanded in water and then transferred to one of three solvents: ethanol, isopropanol, or acetone (Figs. 6–8). Inspection of the eosin-stained specimens (Figs. 6–8 A) reveals that the stain diffuses evenly throughout the samples, effectively overcoming tropoelastin's autofluorescence and enabling fluorescence imaging of surface features. Photographs of the gels taken at different stages of the expansion process - after embedding, after expansion in water, and after changing the expansion solvent (Figs. 6–8 B) - show that the gels containing the stained tropoelastin sample reproduced the behavior previously observed for DMAA gels as disks in various solvents (Fig. 2). The expansion factors obtained by measuring the dimensions of the gels were 2.0 ± 0.1-fold in water, 1.9 ± 0.3-fold in ethanol, 1.9 ± 0.2-fold in isopropanol, and 1.6 ± 0.1-fold in acetone. The corresponding values obtained from quantitative analysis of the microscopy images were in close agreement, yielding 2.0 ± 0.1-fold for both water and ethanol, 1.9 ± 0.1-fold for isopropanol, and 1.6 ± 0.1-fold for acetone.

To assess the impact of the protocol on sample visualization, we performed fluorescence microscopy at each stage of the expansion process (Figs. 6–8 C-K). In its pristine, unexpanded state, the eosin-stained tropoelastin fleece exhibits a relatively uniform fluorescence and poorly defined structural features, as shown in the overview micrographs (Figs. 6–8 C), which become more apparent in the magnified

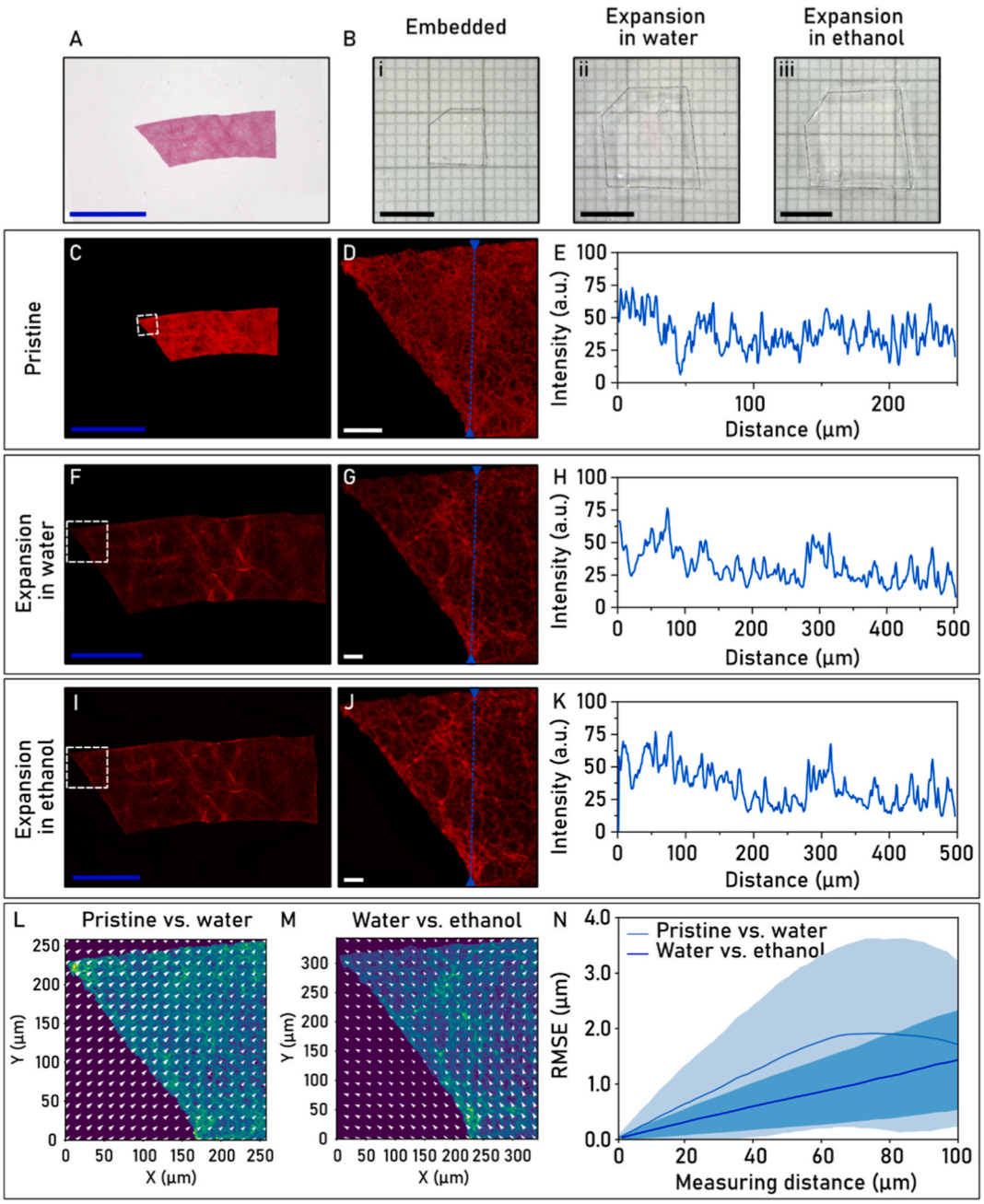

Fig. 6. Stepwise expansion and distortion analysis of an electrospun tropoelastin fleece treated with ethanol. (A) Bright-field micrograph of the eosin-stained tropoelastin fleece prior to hydrogel embedding. (B) Photographs showing the three stages of the expansion process: (i) fleece embedded in the gel, (ii) after the first expansion in water and (iii) after subsequent expansion step in ethanol. Dotted lines indicate the gel edges. Fluorescence micrographs at each stage: (C, D) before expansion, with (E) the corresponding intensity profile measured along the dotted blue lines in (D); (F, G) after expansion in water, with (H) the corresponding intensity profile for the water expanded state in (G); (I, J) after expansion in ethanol, with (K) the corresponding intensity profile for the ethanol-treated state in (J). (L, M) Displacement vectors illustrate local distortions following expansion in (L) water and (M) ethanol. The root-mean-square error (RMSE) quantifies the average distortion magnitude for each state. Shaded regions indicate 1 σ standard deviation. Scale bars: 0.5 cm (black); 1000 µm (blue); 50 µm (white). (For interpretation of the references to color in this figure legend, the reader is referred to the Web version of this article.)

view (Figs. 6–8 D). The corresponding intensity profile along the indicated line is characterized by high-frequency low-amplitude fluctuations (Figs. 6–8 E). The first expansion step in water consistently improved visualization by physically separating the fibers (Figs. 6–8 F). This resolved the underlying fibrous architecture (Figs. 6–8 G), which is quantitatively demonstrated by the appearance of more distinct peaks and valleys in the intensity profiles of the water-expanded samples (Figs. 6–8 H), which now shows more distinct peaks and valleys corresponding to the fibers. The subsequent solvent exchange further enhanced image quality, primarily by increasing contrast. For the ethanol-treated sample, the intensity profile became notably sharper than in its water-expanded state, indicating a superior resolution of the individual fibers (Fig. 6 K *vs.* 6 H). Similar contrast enhancement was observed for isopropanol (Fig. 7 I and J), which exhibited more pronounced intensity fluctuations compared to the pristine sample (Fig. 7 E). Imaging of acetone-expanded samples (Fig. 8 I and J) and the corresponding line profile (Fig. 8K) confirmed that imaging in acetone is feasible; however, visual inspection indicates that acetone induces substantial structural distortions. Moreover, issues such as increased sample fragility, incompatibility with materials commonly used to

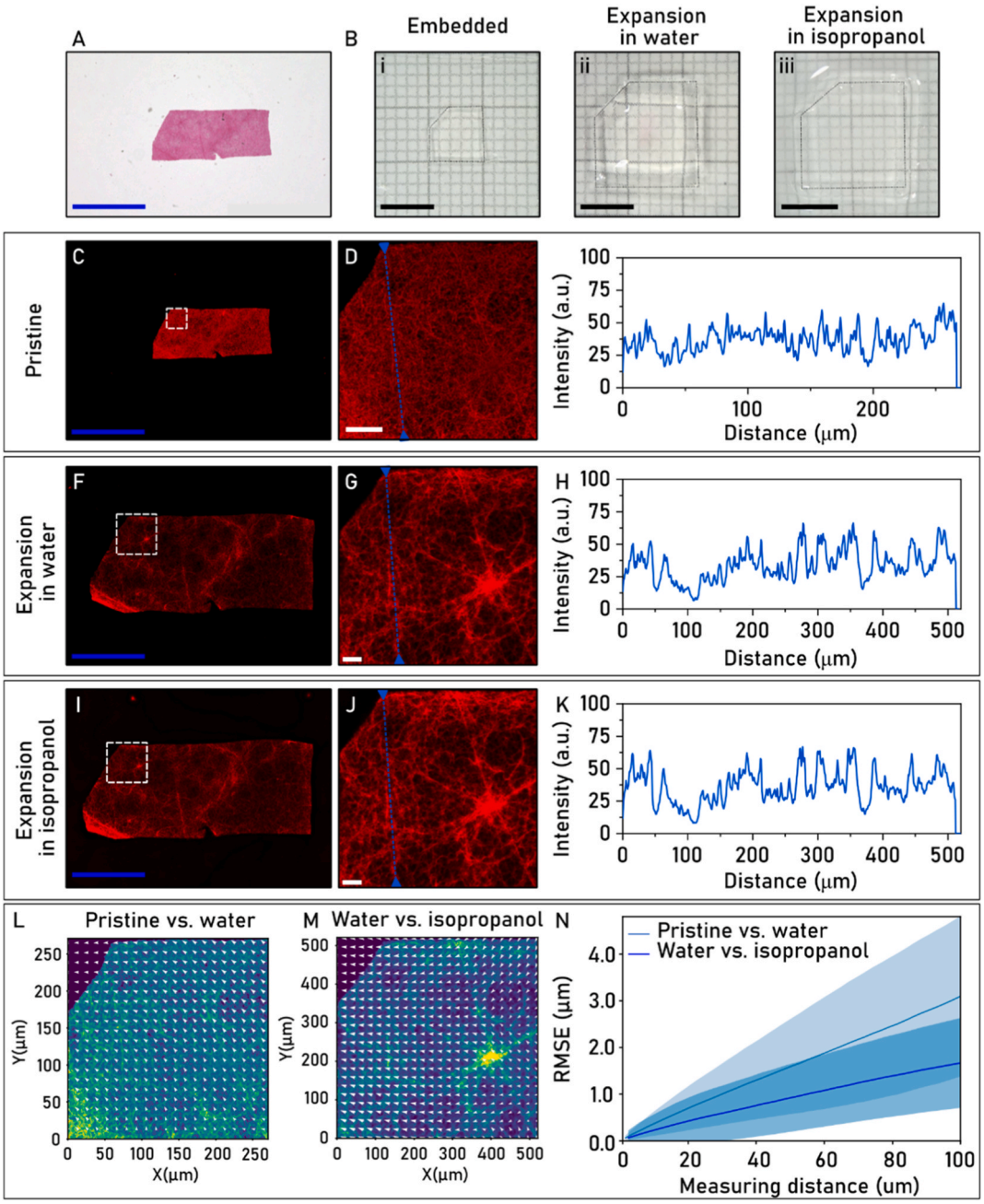

Fig. 7. Stepwise expansion and distortion analysis of an electrospun tropoelastin fleece treated with isopropanol. (A) Bright-field micrograph of the eosin-stained tropoelastin fleece prior to hydrogel embedding. (B) Photographs showing the three stages of the expansion process: (i) fleece embedded in the gel, (ii) after the first expansion in water and (iii) after subsequent expansion step in isopropanol. Dotted lines indicate the gel edges. Fluorescence micrographs at each stage: (C, D) before expansion, with (E) the corresponding intensity profile measured along the dotted blue lines in (D); (F, G) after expansion in water, with (E) the corresponding intensity profile for the water expanded state in (G); (I, J) after expansion in isopropanol, with (K) the corresponding intensity profile for the isopropanol-treated state in (J). (L, M) Displacement vectors illustrate local distortions following expansion in (L) water and (M) isopropanol. The RMSE quantifies the average distortion magnitude for each state. Shaded regions indicate 1 σ standard deviation. Scale bars: 0.5 cm (black); 1000 μm (blue); 50 μm (white). (For interpretation of the references to color in this figure legend, the reader is referred to the Web version of this article.)

mount the samples, and the potential risk of equipment damage render acetone unsuitable for routine imaging applications.

We illustrate local distortions caused by the expansion process using displacement vectors (Figs. 6–8, L and M). We quantified these distortions by calculating the root-mean-square error (RMSE) of the pairwise distances between specific features in the images at each stage (before and after expansion in water, followed by solvent exchange). The RMSE of displacement between the pre-expansion and water-expanded states was found to average below 5.0 μm over a 100 μm length scale (Figs. 6–8 N). This level of precision is consistent with values reported for other leading expansion microscopy protocols [45–47], confirming that the relative arrangement of structural features is well-preserved. It is evident that the distortions introduced during the initial gel expansion were more significant than those arising from the subsequent solvent exchange. General causes for such artifacts include heterogeneity in the polymer network and physical handling of the sample. However, a closer examination of the displacement vector fields (Figs. 6–8 L) suggests that these distortions are not uniformly distributed. The magnitude and directionality of the vectors are more pronounced at the sample peripheries compared to the more random orientation within the sample's

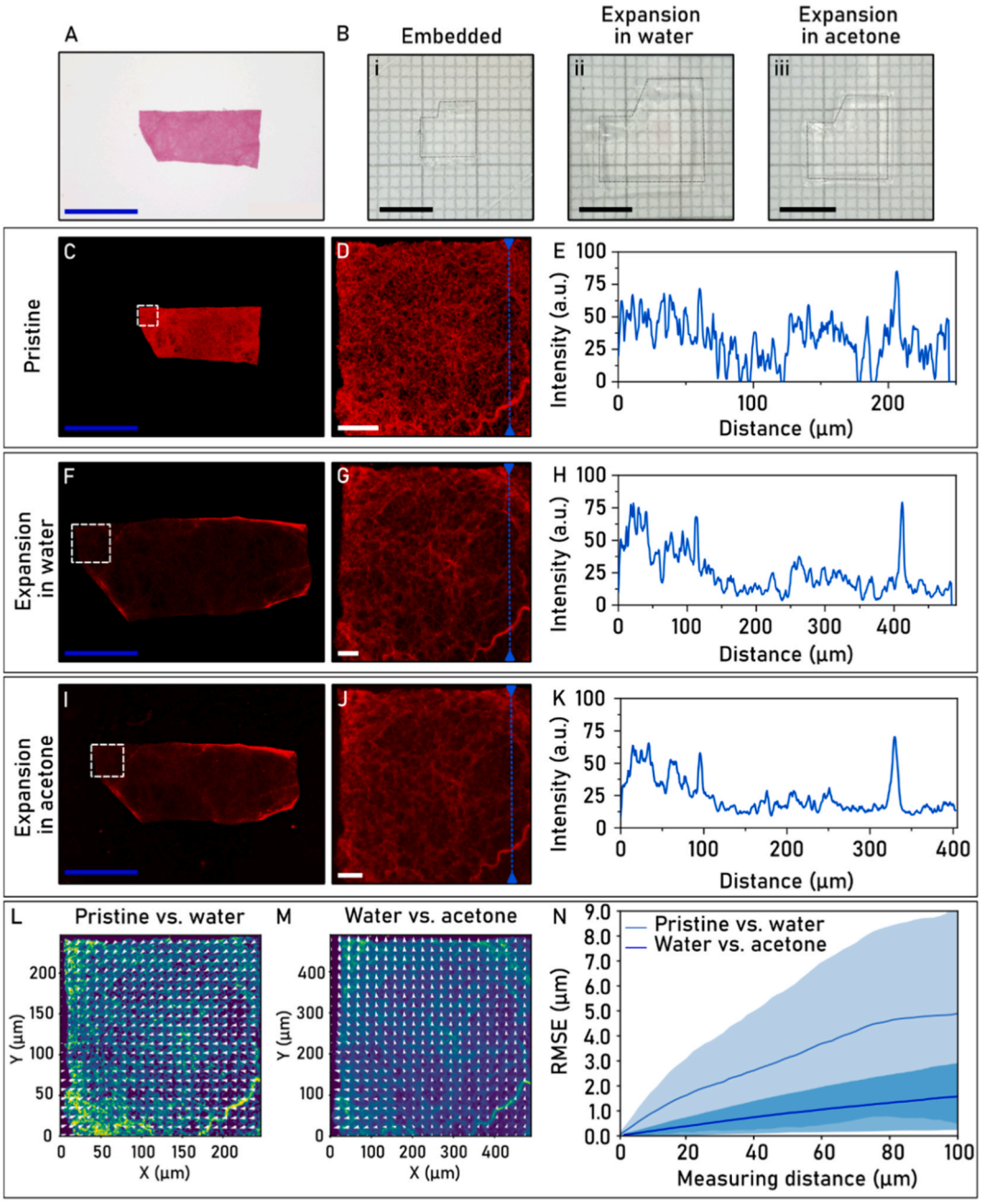

Fig. 8. Stepwise expansion and distortion analysis of an electrospun tropoelastin fleece treated with acetone. (A) Bright-field micrograph of the eosin-stained tropoelastin fleece prior to hydrogel embedding. (B) Photographs showing the three stages of the expansion process: (i) fleece embedded in the gel, (ii) after the first expansion in water and (iii) after subsequent expansion step in acetone. Dotted lines indicate the gel edges. Fluorescence micrographs at each stage: (C, D) before expansion, with (E) the corresponding intensity profile measured along the dotted blue lines in (D); (F, G) after expansion in water, with (E) the corresponding intensity profile for the water expanded state in (G); (I, J) after expansion in acetone, with (K) the corresponding intensity profile for the acetone-treated state in (J). (L, M) Displacement vectors illustrate local distortions following expansion in (L) water and (M) acetone. The RMSE quantifies the average distortion magnitude for each state. Shaded regions indicate 1 σ standard deviation. Scale bars: 0.5 cm (black); 1000 μm (blue); 50 μm (white). (For interpretation of the references to color in this figure legend, the reader is referred to the Web version of this article.)

bulk. This suggests a boundary effect, possibly due to partial detachment of the hydrophobic tropoelastin sample from the glass slide during gel embedding. As these peripheral regions were used for image registration, this may also concentrate calculated error at the sample's boundaries.

The level of distortion introduced by the solvent exchange varies significantly between the three solvents. Ethanol introduces the least distortion and the transition to ethanol demonstrated the highest structural fidelity. The displacement vectors were minimal in magnitude and uniformly oriented (Fig. 6 L and M), resulting in the lowest measured RMSE (compared to other solvents) of around 1.4 ± 0.9 μm over 100 μm distance (Fig. 6 N). Isopropanol introduces moderate, but higher, distortion compared to ethanol, reaching approximately 1.6 ± 1 μm over a 100 μm measuring distance (Fig. 7 N). Acetone causes significant, non-uniform distortions, indicating substantial structural rearrangement and warping of the sample. As a result, acetone features relatively higher RMSE of 1.7 ± 1.5 μm over a 100 μm and the largest standard deviation compared to other solvents (Fig. 8 N).

The measured fluorescence retention rates after expansion were: 21 ± 7 % for water, 9 ± 4 % for ethanol, 37 ± 3 % for isopropanol, and 67 ± 7 % for acetone (Fig. S6). These results indicate that absolute signal intensity is not the primary determinant of image quality in this system, which is best illustrated by the findings with ethanol and acetone. Ethanol, which produced the highest quality images with the lowest structural distortion, also exhibited the lowest fluorescence retention. Conversely, acetone, which yielded the highest retention, caused the most severe imaging artifacts and structural damage. The superior image quality observed in ethanol, despite lower signal retention, may arise from several factors, particularly the near-equivalent expansion observed upon interchange with water. In addition, the lower polarity of ethanol compared to water induces a solvatochromic red shift in the fluorescence emission of eosin, which may further enhance image contrast and signal definition [48]. This spectral shift likely reduces the background signal, thus improving image contrast. The same principle should also apply to other solvents of lower polarity, such as isopropanol. In addition, eosin may undergo dimerization at high local

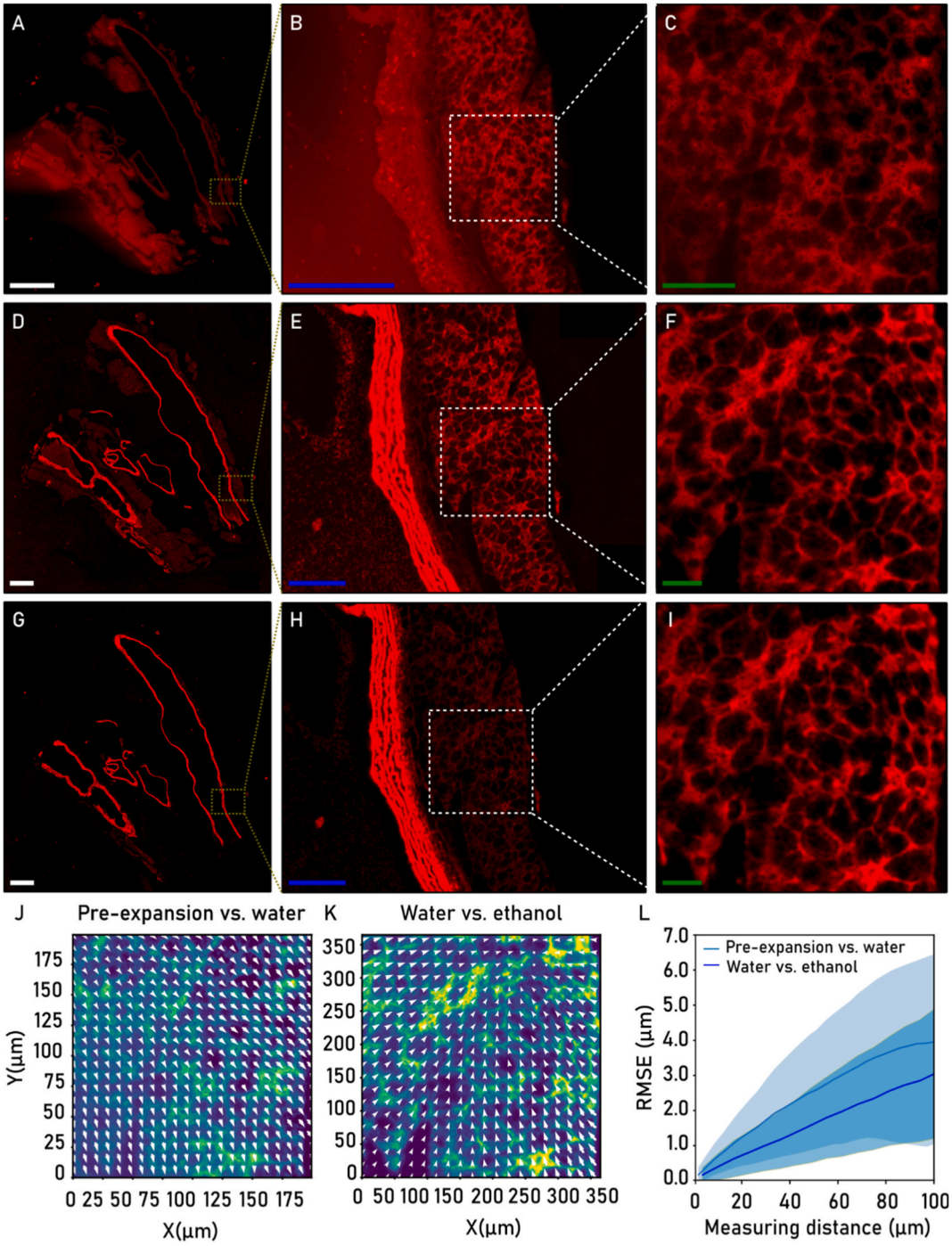

Fig. 9. Stepwise expansion and distortion analysis of mouse aorta. Fluorescence micrographs of the sample: (A) before expansion, with the area highlighted shown magnified in (B) and (C), (D–F) after expansion in water; (G–I) after expansion in ethanol. (J, K) Displacement vectors show the local distortions caused by the expansion process in (J) water and (K) ethanol. Displacement vectors illustrate local distortions following expansion in (J) water and (K) ethanol. The RMSE quantifies the average distortion magnitude for each state. Shaded regions indicate 1 σ standard deviation. Scale bars: 1000 µm (white); 100 µm (blue), 100 µm (green). (For interpretation of the references to color in this figure legend, the reader is referred to the Web version of this article.)

concentrations, particularly in protic solvents such as water, ethanol, and isopropanol, which may also contribute to the varying retention rates and contrast observed.

3.3. Application of the DMAA-based gels for the expansion of mouse aorta sample

Building on the successful validation of our protocol to tropoelastin, we applied the optimized expansion protocol to a more challenging biological sample: aortic tissue (Fig. 9). The primary objective was to physically expand this dense tissue matrix to improve the resolution of its constituent structures in water and ethanol. The protocol yielded a consistent physical expansion by a factor of 1.9 ± 0.2-fold in both solvents and the expansion dramatically improved the visualization of the aorta tissue architecture. Initially, the unexpanded tissue was characterized by dense, overlapping structures with limited detail (Fig. 9 A–C). While the elastic lamina was visible, the surrounding cells remained a diffuse, unresolved fluorescent area. Following expansion in water, these constituent structures became clearly delineated, with a sharply defined elastic lamina and better-resolved structures (Fig. 9 D–F). After being immersed in ethanol (Fig. 9 G), the image quality was maintained, and details appeared sharper and more distinct than in the pre-expansion sample (Fig. 9 H–I).

A key difference of the expansion of aorta tissue compared to our tropoelastin model system was the nature of the expansion. The aorta exhibited non-uniform distortion, as confirmed by an RMSE of ~3.9 μm at a measured distance of 100 μm following expansion in water (Fig. 9 J). After replacing the solvent with ethanol, the displacement fields showed localized hotspots (Fig. 9 K), quantitatively confirmed by an RMSE of ~3.0 μm at a measured distance of 100 μm (Fig. 9 L). This anisotropic behavior can be attributed to the aorta's mechanically heterogeneous composition. Thus, while the protocol introduces measurable local distortions, it successfully resolves fine architectural details in a dense, complex tissue that are otherwise obscured.

In this study, we demonstrate that a DMAA-based hydrogel formulation, free of acrylamide and sodium acrylate, enables expansion microscopy (ExM) across multiple organic solvents while maintaining moderate expansion factors and superior mechanical flexibility. We successfully applied this approach to both model tropoelastin fibers and complex murine aortic tissue, achieving enhanced optical resolution through physical sample magnification. To our knowledge, this represents the first multi-solvent-compatible ExM approach that maintains expansion-contraction responsiveness across different solvent environments. The versatility of this system is illustrated by our proof-of-concept demonstration of embedding ethanol-expanded gel samples and tropoelastin fleeces into epoxide-based media (Supplementary Material, Fig. S7), yielding rigid and stable specimens that retained overall expansion despite moderate shrinkage (~20 %) during resin infiltration. Our gels maintain solvent responsiveness and enable direct post-expansion staining in organic solvents - a critical capability for contrast agents that preferentially dissolve in non-aqueous media and would be incompatible with water-swollen or mechanically locked re-embedded hydrogels.

Implementing EM or X-ray imaging on expanded samples requires addressing technical challenges beyond solvent compatibility, including management of reduced contrast agent density after expansion, validation of uniform nanoscale expansion in heavily fixed and stained tissues, and systematic optimization of post-expansion staining protocols. Our DMAA-based gel system provides a foundational capability by enabling direct expansion in organic solvents, simplifying integration with established staining workflows that require non-aqueous environments. This positions our method as an enabling intermediate step toward correlative expansion microscopy across multiple high-resolution imaging platforms.

Several avenues exist for the optimization and extension of this work. While our current protocol involves a 6-h gelation, our results suggest this could be safely reduced to approximately 1 h to meet higher throughput demands. The primary goal for future development will be to increase the expansion factor beyond the current ~2-fold limit while preserving structural integrity. This could be achieved by implementing strategies such as incorporating alternative crosslinkers, utilizing multiple embedding rounds and optimized monomer ratios [5,49], and exploring novel solvent-compatible monomers to reach expansion factors as those reported in studies with similar gel chemistries based in DMAA [6,10,24,50]. Systematic evaluation of the retention and stability of fluorescent markers and fluorescence-tagged antibodies throughout the expansion and embedding processes will be crucial. Leveraging well-characterized reference structures, such as tubulin networks, to assess local expansion factors will further enable quantitative evaluation of isotropy and structural fidelity. Moreover, extending these studies to imaging modalities for which expansion microscopy has not yet been demonstrated, especially those requiring resin embedding or non-aqueous environments, will help to define the full scope and transformative potential of this method across diverse research fields.

4. Conclusions

This study introduces a novel dimethylacrylamide (DMAA)-based hydrogel for expansion microscopy, specifically engineered for compatibility with a range of organic solvents. By systematically optimizing monomer and crosslinker concentrations, we developed a formulation that offers moderate (1.6 to 2.0-fold) linear expansion, but consistent across aqueous and organic media, along with high flexibility for improved sample handling. We demonstrated that this hydrogel is highly compatible with a conventional histological stain, eosin Y, first validating the protocol on a model tropoelastin scaffold. The true utility of the method was then showcased on dense aortic tissue. Despite the tissue's inherent mechanical heterogeneity inducing a measurable anisotropic distortion in water of 3.9 μm in a 100 μm range, the protocol achieved a 2-fold physical expansion compatible with that of the native gel, enabling the visualization of fine architectural details. This work therefore provides a robust and accessible tool that substantially broadens the applicability of ExM, enabling researchers to investigate the microscale organization of complex tissues within workflows that benefit from low yet controllable expansion factors, or that require compatibility with organic solvents, such as those involving epoxy resin embedding. Future efforts will focus on achieving higher expansion factors and validating the approach across additional microscopy techniques and a broader range of samples, thereby opening new possibilities for high-resolution biological imaging.

CRediT authorship contribution statement

Murilo Izidoro Santos: Writing – review & editing, Writing – original draft, Methodology, Investigation, Formal analysis, Data curation, Conceptualization. **Zviadi Katcharava:** Writing – review & editing, Investigation, Conceptualization. **Prerak Dhawan:** Writing – original draft, Software, Formal analysis. **Tobias Hedkte:** Writing – review & editing, Investigation, Conceptualization. **Wolfgang H. Binder:** Writing – review & editing, Resources, Conceptualization. **Christian E.H. Schmelzer:** Writing – review & editing, Resources, Conceptualization. **Sébastien Blaise:** Writing – review & editing, Resources. **Ralf B. Wehrspohn:** Writing – review & editing, Resources, Conceptualization. **Juliana Martins de Souza e Silva:** Writing – review & editing, Writing – original draft, Validation, Supervision, Methodology, Formal analysis, Conceptualization.

Declaration of generative AI and AI-assisted technologies in the writing process

During the preparation of this work the authors used GPT-4o (OpenAI), Gemini 2.5 Pro (Google), and R1 Distill Llama 70B

(DeepSeek) to improve the language and readability of the manuscript. Having used these tools, the authors reviewed and edited the content as needed, taking full responsibility for the content of the published article.

Declaration of competing interest

The authors declare that they have no known competing financial interests or personal relationships that could have appeared to influence the work reported in this paper.

Acknowledgements

We kindly thank Franziska Seifert (Institute of Pharmacy - MLU) for providing the tropoelastin and Werner Petzold (Fraunhofer IMWS) for electrospinning of it and preparing the histological cuts of the aorta. This research did not receive any specific grant from funding agencies in the public, commercial, or not-for-profit sectors.

Appendix A. Supplementary data

Supplementary data to this article can be found online at https://doi.org/10.1016/j.mtadv.2025.100666.

Data availability

Data will be made available on request.

References

[1] F. Chen, P.W. Tillberg, E.S. Boyden, Expansion microscopy, Science 347 (2015) 543–548, https://doi.org/10.1126/science.1260088.
[2] R. Gao, S.M. Asano, E.S. Boyden, Q & A: expansion microscopy, BMC Biol. 15 (2017) 1–9, https://doi.org/10.1186/s12915-017-0393-3.
[3] A. Klimas, Y. Zhao, Expansion microscopy: toward nanoscale imaging of a diverse range of biomolecules, ACS Nano 14 (2020) 7689–7695, https://doi.org/10.1021/acsnano.0c04374.
[4] E. Abbe, Beiträge zur Theorie des Mikroskops, Arch. Mikrosk. Anat. 9 (1873) 413–468, https://doi.org/10.1007/BF02956173, 413–468.
[5] J.-B. Chang, F. Chen, Y.-G. Yoon, E.E. Jung, H. Babcock, J.S. Kang, S. Asano, H.-J. Suk, N. Pak, P.W. Tillberg, A.T. Wassie, D. Cai, E.S. Boyden, Iterative expansion microscopy, Nat. Methods 14 (2017) 593–599, https://doi.org/10.1038/nmeth.4261.
[6] A. Klimas, B.R. Gallagher, P. Wijesekara, S. Fekir, E.F. DiBernardo, Z. Cheng, D. B. Stolz, F. Cambi, S.C. Watkins, S.L. Brody, A. Horani, A.L. Barth, C.I. Moore, X. Ren, Y. Zhao, Magnify is a universal molecular anchoring strategy for expansion microscopy, Nat. Biotechnol. 41 (2023) 858–869, https://doi.org/10.1038/s41587-022-01546-1.
[7] S.P. Pernal, A. Liyanaarachchi, D.L. Gatti, B. Formosa, R. Pulvender, E.R. Kuhn, R. Ramos, A.R. Naik, K. George, S. Arslanturk, D.J. Taatjes, B.P. Jena, Nanoscale imaging using differential expansion microscopy, Histochem, Cell Biol. 153 (2020) 469–480, https://doi.org/10.1007/s00418-020-01869-7.
[8] S. Truckenbrodt, C. Sommer, S.O. Rizzoli, J.G. Danzl, A practical guide to optimization in X10 expansion microscopy, Nat. Protoc. 14 (2019) 832–863, https://doi.org/10.1038/s41596-018-0117-3.
[9] S. Park, X. Wang, X. Li, X. Huang, K.C. Fong, C. Yu, A.A. Tran, L. Scipioni, Z. Dai, L. Huang, X. Shi, Proximity labeling expansion microscopy (PL-ExM) resolves structure of the interactome (Preprint), bioRxiv (2023), https://doi.org/10.1101/2023.11.09.566477.
[10] S. Wang, T.W. Shin, H.B. Yoder 2nd, R.B. McMillan, H. Su, Y. Liu, C. Zhang, K. S. Leung, P. Yin, L.L. Kiessling, E.S. Boyden, Single-shot 20-fold expansion microscopy, Nat. Methods 21 (2024) 2128–2134, https://doi.org/10.1038/s41592-024-02454-9.
[11] C.G. Galbraith, J.A. Galbraith, Super-resolution microscopy at a glance, J. Cell Sci. 124 (2011) 1607–1611, https://doi.org/10.1242/jcs.080085.
[12] P.W. Tillberg, F. Chen, K.D. Piatkevich, Y. Zhao, C.C. Yu, B.P. English, L. Gao, A. Martorell, H.J. Suk, F. Yoshida, E.M. Degennaro, D.H. Roossien, G. Gong, U. Seneviratne, S.R. Tannenbaum, R. Desimone, D. Cai, E.S. Boyden, Protein-retention expansion microscopy of cells and tissues labeled using standard fluorescent proteins and antibodies, Nat. Biotechnol. 34 (2016) 987–992, https://doi.org/10.1038/nbt.3625.
[13] T. Ku, J. Swaney, J.Y. Park, A. Albanese, E. Murray, J. Hun Cho, Y.G. Park, V. Mangena, J. Chen, K. Chung, Multiplexed and scalable super-resolution imaging of three-dimensional protein localization in size-adjustable tissues, Nat. Biotechnol. 34 (2016) 973–981, https://doi.org/10.1038/nbt.3641.
[14] R. Gao, C.J. Yu, L. Gao, K.D. Piatkevich, R.L. Neve, J.B. Munro, S. Upadhyayula, E. S. Boyden, A highly homogeneous polymer composed of tetrahedron-like monomers for high-isotropy expansion microscopy, Nat. Nanotechnol. 16 (2021) 698–707, https://doi.org/10.1038/s41565-021-00875-7.
[15] D. Gambarotto, F.U. Zwettler, M. Le Guennec, M. Schmidt-Cernohorska, D. Fortun, S. Borgers, J. Heine, J.-G. Schloetel, M. Reuss, M. Unser, E.S. Boyden, M. Sauer, V. Hamel, P. Guichard, Imaging cellular ultrastructures using expansion microscopy (U-ExM), Nat. Methods 16 (2019) 71–74, https://doi.org/10.1038/s41592-018-0238-1.
[16] O. M'Saad, J. Bewersdorf, Light microscopy of proteins in their ultrastructural context, Nat. Commun. 11 (2020) 3850, https://doi.org/10.1038/s41467-020-17523-8.
[17] D.E. Sun, X. Fan, Y. Shi, H. Zhang, Z. Huang, B. Cheng, Q. Tang, W. Li, Y. Zhu, J. Bai, W. Liu, Y. Li, X. Wang, X. Lei, X. Chen, Click-ExM enables expansion microscopy for all biomolecules, Nat. Methods 18 (2021) 107–113, https://doi.org/10.1038/s41592-020-01005-2.
[18] C. Mao, M.Y. Lee, J.-R. Jhan, A.R. Halpern, M.A. Woodworth, A.K. Glaser, T. J. Chozinski, L. Shin, J.W. Pippin, S.J. Shankland, J.T.C. Liu, J.C. Vaughan, Feature-rich covalent stains for super-resolution and cleared tissue fluorescence microscopy, Sci. Adv. 6 (2020) eaba4542, https://doi.org/10.1126/sciadv.aba4542.
[19] S.M. Asano, R. Gao, A.T. Wassie, P.W. Tillberg, F. Chen, E.S. Boyden, Expansion microscopy: protocols for imaging proteins and RNA in cells and tissues, Curr. Protoc. Mol. Biol. 80 (2018) 1–41, https://doi.org/10.1002/cpcb.56.
[20] G. Wen, M. Vanheusden, A. Acke, D. Valli, R.K. Neely, V. Leen, J. Hofkens, Evaluation of direct grafting strategies via trivalent anchoring for enabling lipid membrane and cytoskeleton staining in expansion microscopy, ACS Nano 14 (2020) 7860–7867, https://doi.org/10.1021/acsnano.9b09259.
[21] E.L. Faulkner, S.G. Thomas, R.K. Neely, An introduction to the methodology of expansion microscopy, Int. J. Biochem. Cell Biol. 124 (2020), https://doi.org/10.1016/j.biocel.2020.105764, 105764-105764.
[22] Y. Hu, X. Chu, T.-t. Chen, Q. Pan, C. Liu, J. Yi, X. Chu, Improving resolving ability of expansion microscopy by varying crosslinker concentration, Chem. Commun. 56 (2020) 4176–4179, https://doi.org/10.1039/D0CC00052C.
[23] E.S. Boyden, N. Obidin, R. Gao, L. Gao, Dimethylacrylamide (DMAA) hydrogel for expansion microscopy (ExM). US 2021/0196856 A1, Available at: https://patents.google.com/patent/US20210196856A1/en, 2021.
[24] S. Truckenbrodt, M. Maidorn, D. Crzan, H. Wildhagen, S. Kabatas, S.O. Rizzoli, X10 expansion microscopy enables 25-nm resolution on conventional microscopes, EMBO Rep. 19 (2018), https://doi.org/10.15252/embr.201845836.
[25] A.H. Shaib, A.A. Chouaib, R. Chowdhury, J. Altendorf, D. Mihaylov, C. Zhang, D. Krah, V. Imani, R.K.W. Spencer, S.V. Georgiev, N. Mougios, M. Monga, S. Reshetniak, T. Mimoso, H. Chen, P. Fatehbasharzad, D. Crzan, K.A. Saal, M. M. Alawieh, N. Alawar, J. Eilts, J. Kang, A. Soleimani, M. Muller, C. Pape, L. Alvarez, C. Trenkwalder, B. Mollenhauer, T.F. Outeiro, S. Koster, J. Preobraschenski, U. Becherer, T. Moser, E.S. Boyden, A.R. Aricescu, M. Sauer, F. Opazo, S.O. Rizzoli, One-step nanoscale expansion microscopy reveals individual protein shapes, Nat. Biotechnol. (2024), https://doi.org/10.1038/s41587-024-02431-9.
[26] H. Kamogawa, T. Sekiya, Crosslinking of copolymers of N-methylolacrylamide and ethyl acrylate induced by heat treatment, J. Polym. Sci. 50 (1961) 211–225, https://doi.org/10.1002/pol.1961.1205015322.
[27] B.H. Cipriano, S.J. Banik, R. Sharma, D. Rumore, W. Hwang, R.M. Briber, S. R. Raghavan, Superabsorbent hydrogels that are robust and highly stretchable, Macromolecules 47 (2014) 4445–4452, https://doi.org/10.1021/ma500882n.
[28] S. Truckenbrodt, M. Maidorn, D. Crzan, H. Wildhagen, S. Kabatas, S.O. Rizzoli, X10 expansion microscopy enables 25-nm resolution on conventional microscopes, EMBO Rep. 19 (2018), https://doi.org/10.15252/embr.201845836.
[29] A. Valdebenito, M.V. Encinas, Effect of solvent on the free radical polymerization of N,N-dimethylacrylamide, Polym. Int. 59 (2010) 1246–1251, https://doi.org/10.1002/pi.2856.
[30] R.P. Xian, J. Brunet, Y. Huang, W.L. Wagner, P.D. Lee, P. Tafforeau, C.L. Walsh, A closer look at high-energy X-ray-induced bubble formation during soft tissue imaging, J. Synchrotron Radiat. 31 (2024) 566–577, https://doi.org/10.1107/s160057752400290x.
[31] F. Chen, A.T. Wassie, A.J. Cote, A. Sinha, S. Alon, S. Asano, E.R. Daugharthy, J. B. Chang, A. Marblestone, G.M. Church, A. Raj, E.S. Boyden, Nanoscale imaging of RNA with expansion microscopy, Nat. Methods 13 (2016) 679, https://doi.org/10.1038/nmeth.3899.
[32] J.B. Chang, F. Chen, Y.G. Yoon, E.E. Jung, H. Babcock, J.S. Kang, S. Asano, H. J. Suk, N. Pak, P.W. Tillberg, A.T. Wassie, D.W. Cai, E.S. Boyden, Iterative expansion microscopy, Nat. Methods 14 (2017) 593, https://doi.org/10.1038/Nmeth.4261.
[33] T. Hedtke, M. Mende, H. Steenbock, J. Brinckmann, M. Menzel, W. Hoehenwarter, M. Pietzsch, T. Groth, C.E.H. Schmelzer, Fabrication of insoluble elastin by enzyme-free cross-linking, Macromol. Biosci. 23 (2023), https://doi.org/10.1002/mabi.202300203.
[34] C. Santos de Oliveira, A.T. Gonzalez, T. Hedtke, T. Kurbitz, A. Heilmann, C.E. H. Schmelzer, S.E.S.J. Martins de, Direct three-dimensional imaging for morphological analysis of electrospun fibers with laboratory-based Zernike X-ray phase-contrast computed tomography, Mater. Sci. Eng. C Mater. Biol. Appl. 115 (2020) 111045, https://doi.org/10.1016/j.msec.2020.111045.
[35] C. Reichardt, T. Welton, Empirical parameters of solvent polarity, in: Solvents and Solvent Effects in Organic Chemistry, Wiley-VCH Verlag, 2010, pp. 425–508.
[36] A. Gaudreau-Lapierre, K. Mulatz, J.-C. Béïque, L. Trinkle-Mulcahy, Expansion microscopy-based imaging of nuclear structures in cultured cells, STAR Protoc 2 (2021) 100630, https://doi.org/10.1016/j.xpro.2021.100630.

[37] Z. Shao, Q. Liu, Independent characterization of the elastic and the mixing parts of hydrogel osmotic pressure, Extreme Mech. Lett. 64 (2023) 102085, https://doi.org/10.1016/j.eml.2023.102085.
[38] M. Dutkiewicz, Classification of organic solvents based on correlation between dielectric β parameter and empirical solvent polarity parameter E, J. Chem. Soc. Faraday Trans. 86 (1990) 2237–2241, https://doi.org/10.1039/FT9908602237.
[39] F. Wang, X. Yong, J. Deng, Y. Wu, Poly(N,N-dimethylacrylamide-octadecyl acrylate)-clay hydrogels with high mechanical properties and shape memory ability, RSC Adv. 8 (2018) 16773–16780, https://doi.org/10.1039/C8RA01167B.
[40] M. Par, L. Gotovac, S. Horvat, D. Marovic, Z. Tarle, T.T. Tauböck, T. Attin, L. Ratkovski, V. Panduric, Comparing ISO 4049 and Fourier-transform infrared spectroscopy for assessing ambient light sensitivity in dental resin composites, Sci. Rep. 15 (2025) 8455, https://doi.org/10.1038/s41598-025-93088-0.
[41] Z. Li, C. Yu, H. Kumar, X. He, Q. Lu, H. Bai, K. Kim, J. Hu, The effect of crosslinking degree of hydrogels on hydrogel adhesion, Gels 8 (2022), https://doi.org/10.3390/gels8100682.
[42] S. Alfei, F. Pintaudi, G. Zuccari, Synthesis and characterization of amine and aldehyde-containing copolymers for enzymatic crosslinking of gelatine, Int. J. Mol. Sci. 25 (2024) 2897, https://doi.org/10.3390/ijms25052897.
[43] A. Kathiravan, V. Anbazhagan, M.A. Jhonsi, R. Renganathan, A study on the fluorescence quenching of eosin by certain organic dyes, Z. Phys. Chem. 222 (2008) 1013–1021, https://doi.org/10.1524/zpch.2008.5267.
[44] A.A. Waheed, K.S. Rao, P.D. Gupta, Mechanism of dye binding in the protein assay using eosin dyes, Anal. Biochem. 287 (2000) 73–79, https://doi.org/10.1006/abio.2000.4793.
[45] J.H. Day, C.M. Della Santina, P. Maretich, A.L. Auld, K.K. Schnieder, T. Shin, E. S. Boyden, L.A. Boyer, High-throughput expansion microscopy enables scalable super-resolution imaging, eLife 13 (2024), https://doi.org/10.7554/eLife.96025.RP96025.
[46] A. Klimas, B.R. Gallagher, P. Wijesekara, S. Fekir, E.F. DiBernardo, Z. Cheng, D. B. Stolz, F. Cambi, S.C. Watkins, S.L. Brody, A. Horani, A.L. Barth, C.I. Moore, X. Ren, Y. Zhao, Magnify is a universal molecular anchoring strategy for expansion microscopy, Nat. Biotechnol. 41 (2023) 858–869, https://doi.org/10.1038/s41587-022-01546-1.
[47] Y. Zhao, O. Bucur, H. Irshad, F. Chen, A. Weins, A.L. Stancu, E.-Y. Oh, M. DiStasio, V. Torous, B. Glass, I.E. Stillman, S.J. Schnitt, A.H. Beck, E.S. Boyden, Nanoscale imaging of clinical specimens using pathology-optimized expansion microscopy, Nat. Biotechnol. 35 (2017) 757–764, https://doi.org/10.1038/nbt.3892.
[48] M. Chakraborty, A.K. Panda, Spectral behaviour of eosin Y in different solvents and aqueous surfactant media, Spectrochim. Acta Mol. Biomol. Spectrosc. 81 (2011) 458–465, https://doi.org/10.1016/j.saa.2011.06.038.
[49] H. Xu, Q. Xia, L. Chen, A. Wang, X. Liu, Q. Chen, H. Lv, T. Cai, Q. Li, H. Li, Z. Yan, J. Lu, S. Hao, G. Lu, J. Qin, Cyclic expansion microscopy: expanding biological tissue through multiple cycles for ultrastructure imaging (preprint), Res. Sq. (2022), https://doi.org/10.21203/rs.3.rs-1984380/v1.
[50] H.G.J. Damstra, B. Mohar, M. Eddison, A. Akhmanova, L.C. Kapitein, P.W. Tillberg, Visualizing cellular and tissue ultrastructure using Ten-fold robust expansion microscopy (TREx), eLife 11 (2022) e73775, https://doi.org/10.7554/eLife.73775.